UC Berkeley
UC Berkeley Previously Published Works

Title
Imaging of plant current pathways for non-invasive root Phenotyping using a newly developed electrical current source density approach

Authors
Peruzzo, Luca
Chou, Chunwei
Wu, Yuxin
et al.

Imaging of plant current pathways for non-invasive root Phenotyping using a newly developed electrical current source density approach

Luca Peruzzo · Chunwei Chou · Yuxin Wu · Myriam Schmutz · Benjamin Mary · Florian M. Wagner · Petr Petrov · Gregory Newman · Elison B. Blancaflor · Xiuwei Liu · Xuefeng Ma · Susan Hubbard

Abstract

Aims The flow of electric current in the root-soil system relates to the pathways of water and solutes, its characterization provides information on the root architecture and functioning. We developed a current source density approach with the goal of non-invasively image the current pathways in the root-soil system.

Methods A current flow is applied from the plant stem to the soil, the proposed geoelectrical approach images the resulting distribution and intensity of the electric current in the root-soil system. The numerical inversion procedure underlying the approach was tested in numerical simulations and laboratory experiments with artificial metallic roots. We validated the method using

---

Responsible Editor: Andrea Schnepf.

L. Peruzzo · C. Chou · Y. Wu · F. M. Wagner · P. Petrov · G. Newman · S. Hubbard
Earth and Environmental Sciences Area, Lawrence Berkeley National Laboratory, California, USA

C. Chou
e-mail: chunweichou@lbl.gov

Y. Wu
e-mail: ywu3@lbl.gov

F. M. Wagner
e-mail: wagner@geo.uni-bonn.de

P. Petrov
e-mail: pvpetrov@lbl.gov

G. Newman
e-mail: ganewman@lbl.gov

S. Hubbard
e-mail: sshubbard@lbl.gov

L. Peruzzo (✉) · M. Schmutz
University Bordeaux Montaigne – BxINP, Pessac, France
e-mail: lperuzzo@lbl.gov

M. Schmutz
e-mail: myriam.schmutz@ipb.fr

B. Mary
Dipartimento di Geoscienze, Università degli Studi di Padova, Padova, Italy
e-mail: benjamin.mary@unipd.it

F. M. Wagner
Institute for Applied Geophysics and Geothermal Energy, RWTH Aachen University, Aachen, Germany

E. B. Blancaflor · X. Liu
Noble Research Institute, LLC, Ardmore, OK, USA

E. B. Blancaflor
e-mail: eblancaflor@noble.org

X. Liu
e-mail: xliu@noble.org

rhizotron laboratory experiments on maize and cotton plants.

Results Results from numerical and laboratory tests showed that our inversion approach was capable of imaging root-like distributions of the current source. In maize and cotton, roots acted as "leaky conductors", resulting in successful imaging of the root crowns and negligible contribution of distal roots to the current flow. In contrast, the electrical insulating behavior of the cotton stems in dry soil supports the hypothesis that suberin layers can affect the mobility of ions and water.

Conclusions The proposed approach with rhizotrons studies provides the first direct and concurrent characterization of the root-soil current pathways and their relationship with root functioning and architecture. This approach fills a major gap toward non-destructive imaging of roots in their natural soil environment.

Keywords Root current pathways · Root imaging · Current source density · Rhizotron · Electrical resistivity tomography · Mise a la masse

Abbreviations

|	
CSD	Current Source Density
iCSD	inversion of Current Source Density
σ_{cr}	radial electric current conductivity of roots
σ_{cl}	longitudinal electric current conductivity of roots
ρ_{med}	electric resistivity distribution of the growing medium.

Introduction

New root phenotyping technological developments are needed to overcome the limitations of traditional destructive root investigation methods, such as soil coring or "shovelomics" (Trachsel et al. 2011). Mancuso (2012) and Atkinson et al. (2019) provide extensive reviews on the methodological advances on non-destructive root phenotyping, including Bioelectrical Impedance Analysis (BIA), planar optodes, geophysical methods, and vibrating probe techniques. These techniques aim to mitigate key limitations of traditional root phenotyping, especially addressing the need for a better and more convenient characterization of the finer roots and root functioning. Advances in non-invasive and in-situ approaches for monitoring of root growth and function over time are needed to

gain insight into the mechanisms underlying root development and response to environmental stressors.

Geophysical methods have been tested to non-destructively image roots in the field. Ground Penetrating Radar (GPR) approaches have been used to detect coarse roots (Guo et al. 2013; Liu et al. 2018). Electrical Resistivity Tomography (ERT) and ElectroMagnetic Induction (EMI) approaches have been used to image and monitor soil resistivity changes associated with the Root Water Uptake (RWU) (Cassiani et al. 2015; Shanahan et al. 2015; Whalley et al. 2017). Recent studies explored the use of multi-frequency Electrical Impedance Tomography (EIT) to take advantage of the root polarizable nature (Weigand and Kemna 2017, 2019).

Despite these advantages, geophysical methods to date share common limitations regarding root characterization. Geophysical methods developed to investigate geological media: in the case of roots they measure the root response as part of the soil response, see Fig. 1a for the ERT acquisition. Because of the natural soil heterogeneity and variability the resolution and signal characteristics of geophysical methods strongly depend on soil type and conditions. As such, interpretation of the root-soil system response is non-unique, hindering the differentiation between roots of close plants and the extraction of specific information about root physiology from the electrical signals.

Unlike geophysical methods, the BIA for root investigation developed to specifically target the impedance of plant tissues, limiting the influence of the growing medium. A practical consequence is that BIA involves the application of sensors (i.e., electrodes) into the plant to enhance the method sensitivity. BIA measures the electrical impedance response of roots at a single frequency (resistance and capacitance methods) or over a range of frequencies (bioelectrical impedance spectroscopy). The measured BIA responses have been used to estimate root characteristics, such as root absorbing area and root mass (Dietrich et al. 2012; Mancuso 2012; Ozier-Lafontaine and Bajazet 2005). Estimation of these root traits is based on assumptions on the electrical properties of roots (see section Current Pathways in Roots). A key assumption is that current travels and distributes throughout the root system before exiting to the soil (Fig. 1b), with no leakage of current into the soil in the proximal root position (Fig. 1c). It is only in the former case, that the BIA signal would be sensitive to root physiology. Despite the physiological relevance of the BIA assumptions and the number of BIA studies, a suitable solution for the
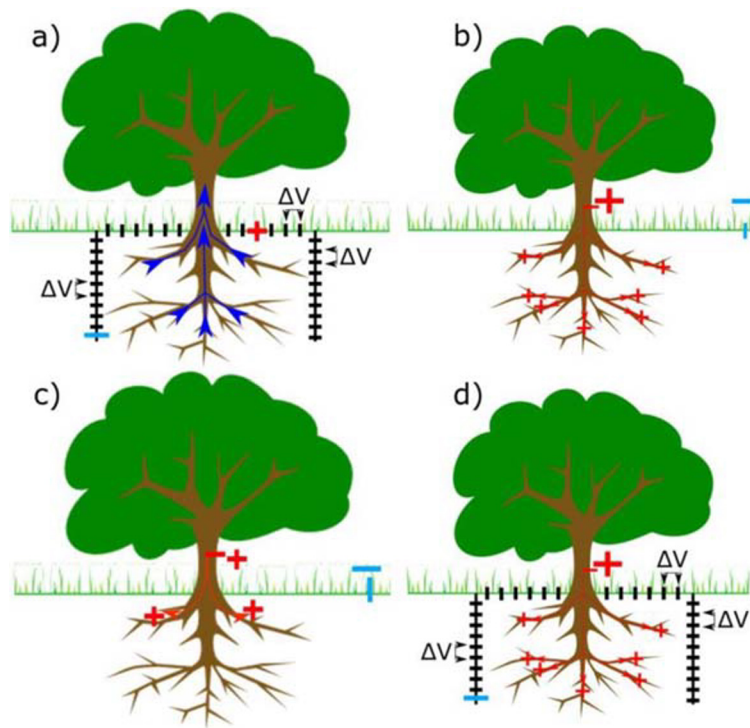
Fig. 1 Electrical approaches for estimating root geometry and functioning. The figures describe the physical conceptualization and electrode positions for the ERT (a), BIA (b, c), and iCSD (d) methods. The red cross and the blue dash are the current injection electrodes. The black dashes are the potential electrodes, used to image the electric potential field (ERT and iCSD). **a**) The ERT method characterizes the RWU through its impact on the soil moisture content and, consequently, on the soil resistivity. **b**) The BIA method investigates root traits based on the impedance response. In this case, since the current flows through the roots before entering the soil, the BIA is sensitive to the roots properties. **c**) In this BIA case, the current passes to the soil without first flowing through the roots. Under these conditions, the BIA is not sensitive to the root properties. **d**) The iCSD method images the positions where the current passes from the plant to the soil (small red crosses) by measuring the distribution of the electric potential

characterization of the current pathways in roots is missing. Thus far, only indirect information obtained from invasive and time-consuming experiments have been available to address this issue (e.g., excavation and trimming).

Mary et al. (2018, 2019), and Mary et al. 2020) tested the combined use of ERT and Mise A La Masse (MALM) methods for imaging grapevine and citrus roots in the field. An approach hereafter called inversion of Current Source Density (iCSD) was used to invert the acquired data. The objective of this inversion approach is to image the density and position of current passing from the plant to the soil. The current source introduced via the stem distributes into "excited" roots that act as a distributed network of current sources (Fig. 1d). Consequently, a spatial numerical inversion of these distributed electric sources provides direct information about the root current pathways and the position of the roots involved in the uptake of water and solutes. The

numerical approach used to invert for the current source density is a key component required for such an approach. Mary et al. (2018) used a nonlinear minimization algorithm for the inversion of the current source density. The algorithm consisted of gradient-based sequential quadratic programming iterative minimization of the objective functions (L1/L2 approach therein) described in Mary et al. (2018). The algorithm was implemented in MATLAB, R2016b, using the *fmincon* method. Because no information about the investigated roots was available, the authors based these inversion assumptions and the interpretation of their results on the available literature data on grapevine root architecture. Consequently, Mary et al. (2018) highlighted the need for further iCSD advances and more controlled studies on the actual relationships between current flow and root architecture.

In this study, we present the methodological formulation and evaluation of the iCSD method, and discuss

its applications for in-situ characterization of current pathways in roots. We perform our studies using laboratory rhizotron experiments on crop roots. The main goals of this study were: 1) develop and test an iCSD inversion code that does not rely on prior assumptions on root architecture and function; 2) design and conduct rhizotron experiments that enable an optimal combination of root visualization and iCSD investigation of the current pathways in roots to provide direct insight on the root electrical behavior and validate the iCSD approach; and 3) perform experiments to evaluate the application of the iCSD method on different plant species (maize and cotton) and growing medium (soil and nutrient solution) that are common to BIA and other plant studies.

Current pathways in roots

The relationship between hydraulic and electrical pathways has been the object of scientific debate because of its physiological relevance and methodological implications for BIA methods (Urban et al. 2011; Dietrich et al. 2012). A key and open question concerns the distribution of the current leakage (i.e., the root portions where the current passes from the root to the soil; Fig. 1b and c). The distribution of the current leakage is controlled by 1) the electrical radial and longitudinal conductivities (σ_{cr} and σ_{cl}), and 2) by the resistivity contrast between root and soil.

With regard to σ_{cr} and σ_{cl}, when σ_{cl} is significantly higher than σ_{cr}, the current will predominantly travel through the xylems to the distal "active" roots, which are mostly root hairs. Based on the link between hydraulic and electrical pathways, this is consistent with a root water uptake (RWU) process where root hairs play a dominant role while the more insulated and suberized roots primarily function as conduits for both water and electric current (Aroca 2012, and references therein). On the contrary, if the σ_{cr} is similar to σ_{cl}, the electrical current does not tend to travel through the entire root system but rather starts leaking into the surrounding medium from root proximal portions. The coexistence of proximal and distal current leakage is in line with studies that suggest the presence of a more diffused zone of RWU, and a more complex and partial insulation effect of the suberization, possibly resulting from the contribution of the cell-to-cell pathways (e.g., Kramer 1946; Steudle 2000; North and Baker 2007; Ranathunge and Schreiber 2011; Schreiber 2010).

Soil resistivity can affect the distribution of the current leakage by influencing the minimum resistance pathways, i.e., whether roots or soil provide the minimum resistance to the current flow. In addition, soil resistivity strongly relates to the soil water content, which, as discussed, affects the root physiology. Therefore, information on the soil resistivity, such as the ERT resistivity imaging, has the potential for supporting the interpretation of both BIA and iCSD results.

Dalton (1995) proposed a model for the interpretation of the plant root capacitance results in which the current equally distributes over the root system. Because of the elongated root geometry this model is coherent with the hypothesis of a low resistance xylem pathway (σ_{cl} > σ_{cr}). Numerous studies have applied Dalton's model documenting the predicted correlation between root capacitance and mass (Dietrich et al. 2012, and references therein). In fact, recent studies with wheat, soy, and maize roots continue to support the capacitance method (Čermák et al. 2013; Preston et al. 2004; Postic and Doussan 2016; Cseresnyés et al. 2018).

Despite accumulating studies supporting the capacitance method, hydroponic laboratory results of Dietrich et al. (2012) and other studies have begun to uncover potential inconsistencies with Dalton's assumptions. In their work, Dietrich et al. (2012) explored the effect of trimming submerged roots on the BIA response and found negligible variation of the root capacitance. Cao et al. (2010) reached similar conclusions regarding the measured electrical root resistance (overall electrical resistance for the electric circuit obtained with injection into the stem and return electrode in the hydroponic solution, Fig. 1a). Urban et al. (2011) discussed the BIA hypotheses and found that the current left the roots in their proximal portion in several of their experiments. Conclusions from the latter study are consistent with the assumption that distal roots have a negligible contribution on root capacitance and resistance.

Because of the complexity of the hydraulic and electrical pathways, their link has long been the object of scientific research and debate. For recent reviews see Aroca (2012) and Mancuso (2012); for previous detailed discussions on pathways in plant cells and tissues see Fensom (1965), Knipfer and Fricke (2010), and Findlay and Hope (1976); see Johnson (2013) and Maherali et al. (2009) in regard to xylem pathways. See Jackson et al. (2000) and Hacke and Sperry (2001) for water pathways in roots. Thus, above discrepancies in the link between electrical and hydraulic root properties can be, at least to some degree, attributed

to differences among plant species investigated and growing conditions.

Among herbaceous plants, maize has been commonly used to investigate root electrical properties (Frensch and Steudle 1989). For instance, Ginsburg (1972) investigated the longitudinal and radial current conductivities (σ_{cl} and σ_{cr}) of excited root segments and concluded that the maize roots behave as leaking conductors. Similarly, Anderson and Higinbotham (1976) found that σ_{cr} of maize cortical sleeves was comparable to the stele σ_{cl}. Recently, Rao et al. (2018) found that maize root conductivity decreases as the root cross-sectional area increases, and that primary roots were more conductive than brace roots. By contrast, BIA studies on woody plants have supported the hypothesis of a radial isolation effect of bark and/or suberized tissues (Čermák et al. 2006; Aubrecht et al. 2006).

Plant growing conditions have been shown to affect both water uptake and solute absorption due to induced differences in root maturation and suberization (e.g., Schreiber 2010). Redjala et al. (2011) observed that the cadmium uptake of maize roots grown in hydroponic conditions was higher than in those grown aeroponically. Tavakkoli et al. (2010) demonstrated that the salt tolerance of barley grown in hydroponic conditions differed from that of soil-grown barley. Zimmermann and Steudle (1998) documented how the development of Casparian bands significantly reduced the water flow in maize roots grown in mist conditions compared to those grown hydroponically. During their investigation on the effect of hypoxia on maize, Enstone and Peterson (2005) reported differences in oxygen flow between plants grown hydroponically and plants grown in vermiculite.

The results reported above and in other investigations (Aroca 2012, and references therein) are conducive to the hypothesis that root current pathways are affected by the growing conditions, as suggested in Urban et al. (2011). For example, the observations by Zimmermann and Steudle (1998) and Enstone and Peterson (2005) may explain the negligible contributions to the BIA signals from distal roots under hydroponic conditions (Cao et al. 2010; Dietrich et al. 2012). At the same time, the more extensive suberization in natural soil and weather conditions could explain the good agreement between the rooting depth reported by Mary et al. (2018) based on the iCSD and the available literature data for grapevines in the field.

To minimize these ambiguities and to develop a more robust approach for non-invasive in-situ root imaging, we aim to develop iCSD inversion code that does not rely on prior assumptions on root architecture and function and use rhizotron experiments to validate the iCSD approach.

Materials and methods

The phrase "inversion of Current Source Density" (iCSD) was introduced by Łęski et al. (2011) to describe the 2D imaging of current sources associated with the brain neural activation. Similar inversion methodologies have been developed for the interpretation of the self-potential data, where the distribution of naturally occurring currents is investigated (Minsley et al. 2007, and references therein). With regard to active methodologies, Binley et al. (1997) developed an analogous approach for detecting pollutant leakage from environmental confinement barriers. Although there are physical and numerical intrinsic differences between application of the iCSD to detect brain neuronal activity and current pathways in roots, we decided to adopt the term iCSD as the general physical imaging of current source density remains valid. With iCSD, we indicate the coupling of ERT and MALM through the proposed numerical inversion procedure for the imaging of the current source density, and its correlation with root architecture.

We introduce the necessary aspects regarding the ERT and MALM methods in this section. However, we direct the interested readers to more in-depth discussion about the ERT method (Binley and Kemna 2005), and to Schlumberger (1920) and Parasnis (1967) with regard to the MALM method.

In the following discussion we use ρ_{med} to represent the 2D or 3D distribution of the electrical resistivity in the growing medium (i.e., hydroponic solution or soil, and with possible influences from RWU and ligneous root mass). CSD represents the 2D, or 3D, distribution of the Current Source Density within the same medium. In the case of roots, the CSD is controlled by the current conduction behavior of the roots, specifically by the leakage pattern of the root system (e.g., proximal or distal current leakage, Fig. 1).

Both ERT and MALM are active methods. In these methods the current is forced through the medium by applying a potential difference between two current electrodes. In ERT, both current electrodes are positioned in the investigated medium, while for MALM the positive current pole is installed in the plant stem,

similar to BIA (Fig. 1). The potential field resulting from the current injection depends on CSD, resistivity of the medium (ρ_{med}), and boundary conditions. The boundary conditions are known a priori and their impact on the potential field can be properly modeled. In ERT, the current sources correspond to the electrodes used to inject current, allowing us to invert for ρ_{med}. Then, the iCSD accounts for the obtained ρ_{med} and explicitly inverts the MALM data to obtain current source distribution.

Laboratory setup and data acquisition

The rhizotrons used in this study were designed to enable the concurrent direct visualization of the roots and electrical measurements. Rhizotron dimensions were 52 cm (x) × 53 cm (y) × 2 cm (z), see Fig. 2. Figure 2a shows the rhizotron setup with 64 silver/silver chloride (Ag/AgCl) electrodes located on the back viewing surface. The viewing surfaces were covered with opaque material to stop the light from affecting the development of the roots. The back viewing surface was removable, allowing homogeneous soil packing for the plant experiments and convenient access to the electrodes. Besides the top opening, the rhizotrons were waterproof to enable hydroponic experiments and controlled evapotranspiration conditions during the soil experiments and plant growth. All the experiments were performed in a growth chamber equipped with automatic growth lights (LumiGrow Pro650e) and controlled temperature and humidity. The temperature varied with a day/night temperature regime of 25/20 °C. The humidity ranged from 45 to 60%.

For both ERT and MALM methods, the electrical potential field is characterized by a set of potential differences (ΔV) measured between pairs of electrodes. It is important to properly arrange the electrodes on the rhizotron viewing surface and design a suitable acquisition sequence to obtain a good sensitivity coverage (hereinafter coverage) of the investigated system (Slater et al. 2002). This is particularly true for the iCSD, as both ERT and MALM acquisitions affect its result.

The 64 electrodes were arranged in a 8 by 8 grid on the back viewing surface of the rhizotron, leaving the front surface clear for the observation (Fig. 2). For the ERT, the designed arrangement of the electrodes offers a good compromise between a high coverage on the central part of the rhizotron, which encompasses the root zone, and a sufficient coverage on the rhizotron sides to avoid an excessive ERT inversion smoothness.

For the MALM, the arrangement of the electrodes is highly sensitive to the position of the investigated current sources. Because of their central positions, the electrodes are closer to the expected sources of current (i.e., the roots) and thus in the region of maximum potential gradient. Hence, this electrode configuration maximizes the changes in both magnitude and sign of the measured ΔV associated with a change in the CSD distribution.

The electrode diameter was 1.5 mm. The penetration of the electrodes into the rhizotron was 4 mm ± 1 mm. To evaluate the possible distorting effects of the densely populated electrodes on the potential field distribution, a test was performed with low conductivity water (20 µS cm^{-1}). The test showed no resistivity anomalies, which may be caused by the presence of the electrodes (data not shown). Therefore, while rhizotron setups with electrodes only on the sides were successfully adopted (Weigand and Kemna 2017), we found that the current setup represents a better solution for iCSD experiments (Fig. 2).

Data were acquired with a MTP DAS-1 resistivity meter with 8 potential channels. For the ERT acquisition over the 2D grid of electrodes, we chose a dipole-dipole skip 2 configuration. For each skip 2-couple of injection electrodes (e.g., electrodes 1 and 4) the remaining skip-2 couples of electrodes were used as potential dipoles (e.g., electrodes 5 and 8, 6 and 9, etc.). The associated complete set of reciprocals was also acquired, the resulting acquisition sequence contained 3904 data points (Binley and Kemna 2005; Parasnis 1988; Mary et al. 2018).

Following the ERT data acquisition, the MALM data acquisition required little setup adjustments and time. As the two current electrodes are fixed, the use of a multichannel resistivity meter significantly reduced the acquisition time and, consequently, supported the acquisition of more robust data sets. Electrode 1 was used to inject the current into the plant stem, while electrode 64 was used as a return electrode in the growing medium (Fig. 1d). The remaining 62 electrodes were used to map the resulting potential field. A sequence with 204 ΔVs was used. Considering the grid in Fig. 2a, the sequence included the vertical, horizontal, and diagonal ΔVs between adjacent electrodes. While 61 ΔVs would provide all the independent differences, the 204 ΔV sequence was preferred because of its redundancy and consequent
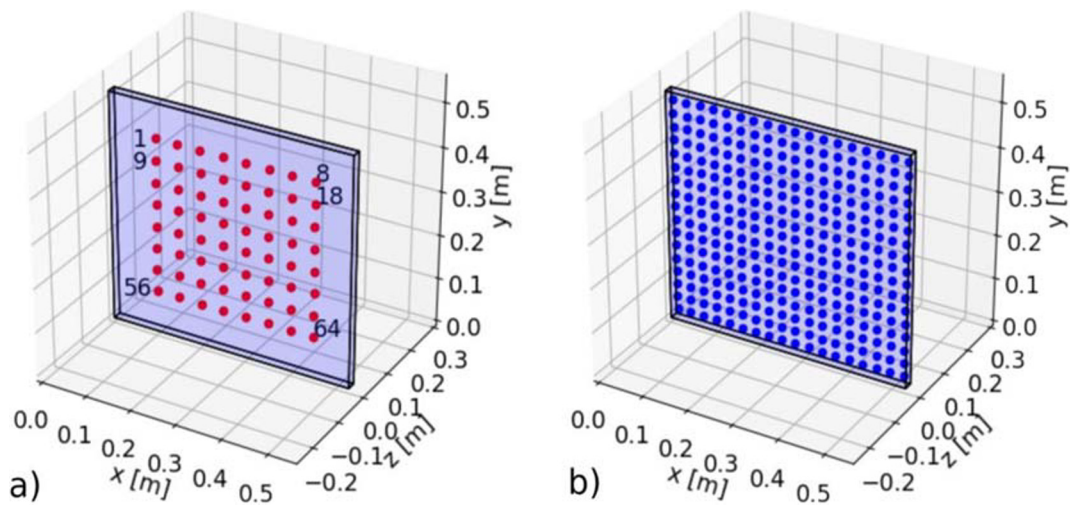
Fig. 2 Rhizotron setup. Dimensions are 53x52x2 cm. a) the 64 silver/silver chloride electrodes were distributed to maximize both ERT and MALM data quality and coverage, thus enhancing the

resolution and stability of the iCSD. b) positions of the VRTe, possible current point sources used for the iCSD

lower sensitivity to acquisition errors. The acquisition time remained relatively short (2–3 min) as the multi-channel instrument was optimized with fixed current electrodes that allowed 8 ΔVs to be measured at once.

Data processing and ERT inversion

ERT and MALM data were filtered considering: 1) reciprocal error (5% threshold), 2) stacking error (3 stacks, 5% error threshold), 3) minimum measured ΔV (minimum 0.5 mV threshold), 4) apparent resistivity (the range changed among different data sets), and 5) maximum electrode contact resistance (30 kohm). The filtering was implemented to enhance the control on the ERT inversion and obtain a reliable ρ_{med} for the successive iCSD inversion.

After the processing, the data were inverted with the BERT inversion software to obtain ρ_{med} (Günther and Rücker 2013; Rücker et al. 2006; Günther et al. 2006). Data error was set to 5% in line with the stacking and reciprocal thresholds used for the data filtering. The regularization was adjusted using the lambda optimization algorithm provided by the BERT software. Generally speaking, a rhizotron is treated as a 2D geometry. However, this bounded and thin geometry leads to some complications into the ERT inversion. Specifically, no-current-flow boundary conditions were set for all the rhizotron surface and the inversion had to be adapted for

the resulting pure Neumann problem (Bochev and Lehoucq 2005). For a higher quality forward calculation, the rhizotron volume was discretized in 3D by extruding a 2D mesh with 5 layers. The discretization allowed the refinement of the mesh near the electrodes while maintaining high mesh quality. At the same time, in order to limit the inversion time and force the inversion to be two-dimensional (x, y), the elements in z direction (resulting from the extruded layers) were grouped together and inverted as a unique variable. This way, a 3D forward calculation was implemented within a 2D inversion (Ronczka 2016).

iCSD inversion

The iCSD inversion that we developed was based on the physical principles of a bounded system in which linearity and charge conservation were applied to decompose the investigated CSD distribution into the sum of point current sources. This provided a discrete representation of the root system portions where the current leaks from the roots into the surrounding medium.

Because of the linearity of the problem, the collective potential field from multiple current sources is the linear combination of their individual potential fields. As such, the measured ΔV can be viewed as and decomposed into the sum of multiple ΔVs from a set of possible current sources. These possible current sources are named

ViRTual electrodes (VRTe). As purely numerical (virtual) electrodes, they are simulated by mesh nodes representing possible current sources, but with no direct correlation with the real (physical) electrodes used during data acquisition. Basically, the VRTe were distributed to represent a grid over which the true CSD distribution is discretized. In order to account for any possible CSD, a 2D grid of 306 VRTe was arranged to cover the entire rhizotron (Fig. 2b).

The charge conservation law implies that the sum of the current fractions associated with the VRTe (hereinafter VRTe weights) has to be equal to the overall injected current, which is provided by the resistivity meter. If we normalize the injected current to be equal to 1, the sum of the VRTe weights has to be 1 as well. Briefly, for Ohm's law, normalizing the current to 1 is equivalent to calculating the resistance, R, from ΔV. Then, the use of R simplifies the presentation of the numerical problem.

Once the VRTe nodes are added to the ERT-based ρ_{med} structure, the potential field associated with each of the VRTes is simulated with BERT. From these simulated potential fields, the same sequence of 204 R is extracted, each corresponding to a single VRTe. Each extracted sequence contains the resistances that would be measured in the laboratory if all the current sources were concentrated at the VRTe point (i.e., VRTe Green's function).

The VRTe weights are the unknowns that the iCSD strives to estimate. Once the VRTe weights are estimated and associated with the respective VRTe coordinates, they provide a discrete visualization of the investigated CSD. The problem of estimating the VRTe weights that decompose the measured R sequence into a sum of the simulated VRTe R sequences is analogous to a linear vector decomposition (Strang 1976), and is expressed by:

$$Ax = b \tag{1}$$

Where $\mathbf{A}$ is a matrix, its columns are the simulated VRTe R sequences; $\mathbf{x}$ is a vector containing the unknown VRTe weights; $\mathbf{b}$ is a vector containing the measured sequence of 204 R. Each row in $\mathbf{A}$ corresponds to the relative R in the acquisition sequence, e.g., $\mathbf{A}_{1,1}$ is the first resistance extracted from the potential field simulated with injection at the first VRTe.

The charge conservation is implemented by appending a row of 1's to $\mathbf{A}$ and a corresponding 1 to the vector $\mathbf{b}$. This forces the sum of the VRTe weights to be equal to 1. A weight of 1000 was used to guarantee the charge conservation; with a lower weight observations and regularization may dominate the charge conservation.

Since the problem is undetermined, a first order spatial regularization is added (Menke 1989). Rows are added to express the differences between adjacent (vertically and horizontally) VRTe, e.g., the row $[1 \ -1 \ \ldots]$ is the difference between the first two VRTe weights. The differences are added for the entire VRTe grid and set to 0 by adding corresponding 0's to $\mathbf{b}$.

Lastly, the trade-off between data misfit and solution regularization is controlled by a diagonal weight matrix $\mathbf{W}$. The numerical routine includes a "pareto" functionality wherein regularization and model-to-measurement fit are traded off while changing the regularization weight, i.e., running the inversion with different regularization weights. The obtained set of solutions can be used to construct the "pareto front" (L-curve), which is a widely accepted way to estimate the optimum regularization weight (Hansen and Dianne 1993). Eq. 2 shows the resulting system $WAx = bW$.

$$
\begin{bmatrix}
w_{obs} & 0 & \cdots & 0 \\
0 & w_{obs} & \cdots & 0 \\
\vdots & \vdots & \ddots & \vdots \\
0 & 0 & \cdots & w_{reg}
\end{bmatrix}
\begin{bmatrix}
S_1R_1 & S_2R_1 & \cdots & S_nR_1 \\
S_1R_2 & S_2R_2 & \cdots & S_nR_2 \\
\vdots & \vdots & \ddots & \vdots \\
S_1R_m & S_2R_m & \cdots & S_nR_m \\
1 & 1 & \cdots & 1 \\
-1 & 1 & \cdots & 0 \\
0 & -1 & \cdots & 0 \\
\vdots & \vdots & \ddots & \vdots \\
0 & 0 & \cdots & 1
\end{bmatrix}
\begin{bmatrix}
S_{1,cf} \\
S_{2,cf} \\
\vdots \\
S_{n,cf}
\end{bmatrix}
=
\begin{bmatrix}
R_{1,meas} \\
R_{2,meas} \\
\vdots \\
R_{3,meas} \\
1 \\
0 \\
0 \\
\vdots \\
0
\end{bmatrix}
\begin{bmatrix}
w_{obs} & 0 & \cdots & 0 \\
0 & w_{obs} & \cdots & 0 \\
\vdots & \vdots & \ddots & \vdots \\
0 & 0 & \cdots & w_{reg}
\end{bmatrix}
\tag{2}
$$

Where S indicates the n VRTe sources, R the m resistances, and w the weights used to control the solution regularization.

Lastly, the solution is further constrained by forcing the linear solver to seek only positive VRTe weights (i.e., inequality constraint), as the negative source of

current is known to correspond uniquely to the return electrode.

The linear problem formulation is conducive to the inversion optimization during the calculation of the pareto front. The calculation time of the Pareto front can be further reduced by code optimization as the calculations that do not depend on the regulation weights can separated from the inversion routine and performed only once during the initialization of the linear problem. The initialization phase includes the processing of the MALM experimental data, forward calculation of the VRTe responses for the given ρ_{med}, inclusion of the continuity constraint, and construction of the matrices.

Continuity constraint, bounded-value constraint, and first-order spatial regularization stabilize the inversion while limiting the impact of the spatial regularization strategy. The impact of the spatial regularization was evaluated by monitoring the relative components of the misfit and the resulting distribution of the current source. In both synthetic and laboratory tests, as well as in plant experiments the iCSD results are often limited to few current sources (Figs. 3, 4, 7, and 9).

Synthetic and experimental iCSD testing

Synthetic numerical and laboratory experimental tests were performed in order to evaluate the capabilities of the setup and inversion routine to couple the ERT and MALM approaches for the iCSD. In the numerical tests

both the true source response and VRTe responses were calculated with BERT.

Figure 3 shows an explanatory numerical test with inversion of a point source, and the associated Pareto front that was used to select the optimum regularization strength. As this first experiment was performed to specifically test the inversion routine, a homogeneous ρ_{med} was used in order to avoid influence from the baseline resistivity distribution complexity.

For the second experiment, the laboratory tests were conducted. Because of the ρ_{med} heterogeneity of any experimental system, these laboratory tests need to include the ERT inversion, and the use of the obtained ρ_{med} as input in the iCSD. The true current sources were obtained using insulated metallic wires inserted into the rhizotron (Fig. 4). The insulating plastic cover was removed at the tips (1 cm, red dots in Fig. 4a) of the metallic wires to obtain the desired current sources. Six experimental tests were performed using different numbers and positions of these current sources. The rhizotron was filled with tap water and left to equilibrate to achieve steady state conditions of water temperature and salinity, thus minimizing ρ_{med} heterogeneity and changes during the experiment. Changes in ρ_{med} during the ERT and MALM acquisition periods would make the ERT-based ρ_{med} less accurate and compromise the iCSD. To make sure ρ_{med} was stable, a second ERT was performed after the MALM acquisition and compared with the initial measurement. The conductivity of the solution was also measured in several locations of the rhizotron with a conductivity meter to validate the
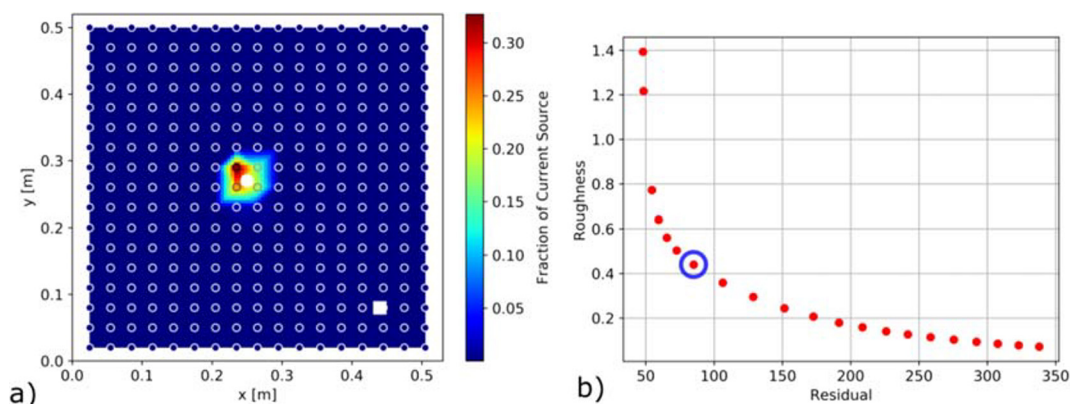
Fig. 3 Numerical synthetic test. a) The synthetic test evaluates the iCSD capability to locate a current point source (white dot). The white circles represent the VRTe and the white square the return electrode. The source of current was centered between four VRTe to highlight the distribution of the current density. While the

fractions of current source refer to the VRTe nodes, the results are linearly interpolated for a better visualization. b) Pareto front used to select the proper regularization weight for the iCSD, the blue-circled inversion was chosen as best compromise between fitting and regularization
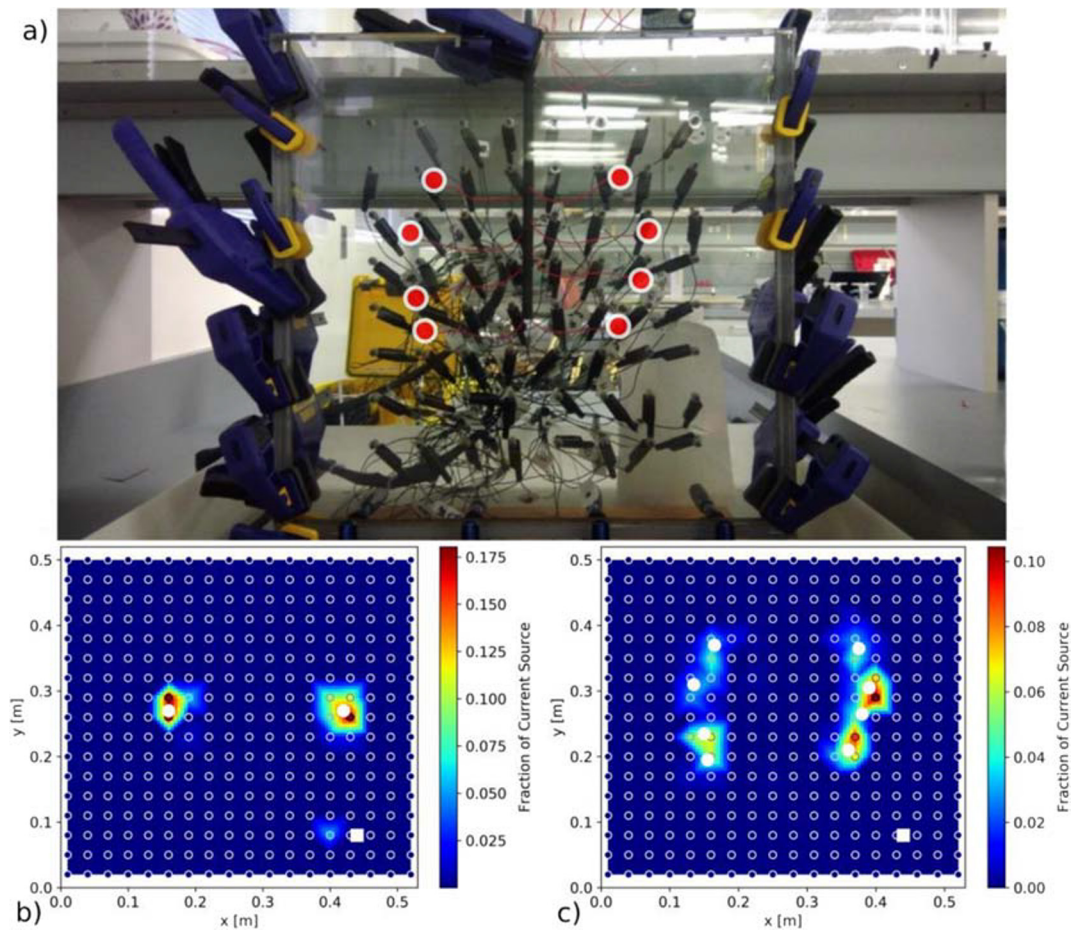
Fig. 4 Laboratory tests. a) Rhizotron filled with water for the tests with metallic wires. The plastic insulation of the metallic wires avoided the current leakage, which occurred only where the insulation was removed (eight red dots). This test simulated a complex and root-like structure, with the current leaking at the tips. b) result of iCSD test with two metallic sources in water. c) result of iCSD

test with eight metallic sources shown in a). In both tests, the unequal distribution of the current among the wires is due to different proximity of the respective sources to the return electrode: the shorter the water path from the source to return electrode, the lower the path resistance, and the bigger the current fraction

ρ_{med} obtained from the ERT inversion. This setup allowed the acquisition of good quality data sets since less than 5% of the data were discharged during the data processing. Because of the controlled laboratory conditions, the ρ_{med} obtained with the ERT was stable and consistent with the direct conductivity measurements. The quality of the ERT inversion was also confirmed by comparing the model responses with the acquired data (i.e. data misfit). Similarly, the acquired iCSD data were plotted against the resistances calculated with the CSD distribution obtained from the iCSD.

The tests also allowed a more informed definition of the VRTe grid. For our setup, a spacing of 3 cm provided a good compromise between resolution, stability, and duration of the iCSD routine. The 3-cm spacing also

agrees with the ERT resolution, which would not support a higher iCSD resolution.

Successive numerical tests were based on the 8-source laboratory tests shown in Fig. 4. These tests aimed to 1) link laboratory and numerical tests to evaluate the influence of the numerical iCSD routine and laboratory setup on the overall iCSD stability and resolution; 2) account for a more complex CSD, given by the 8 wire-tip sources that were used to simulate distal current pathways; and 3) account for possible ρ_{med} heterogeneity. To address goals 1 and 2, the position of the 8 sources was replicated in the numerical tests and a test with homogeneous ρ_{med} was included to simulate the water resistivity of the laboratory tests. To address goal 3, heterogeneous ρ_{med} were tested.
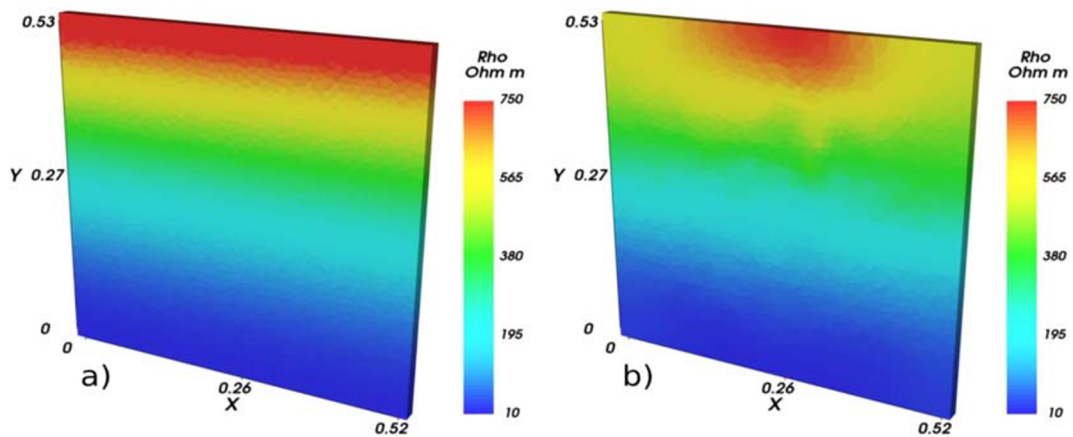
Fig. 5 ERT true resistivity model (**a**) and inverted model (**b**) for the 8-source numerical experiment with quadratic resistivity distribution

In order to account for the heterogeneous ρ_{med} the following modeling steps were carried out. First, a *true* ρ_{med} was assigned to the mesh cells of the rhizotron ERT model. We included homogeneous, linear, and quadratic resistivity profiles in the y direction, see Fig. 5. Second, the ERT acquisition was simulated (i.e., forward calculation) with the ERT laboratory sequence and 3% of Gaussian error, in line with reciprocal and stacking errors observed in the laboratory data sets. Third, the forwarded ERT data sets were inverted following the exact laboratory procedure. A refined and different mesh was used for forward and inverse problems to, respectively, increase the simulation accuracy and avoid the *inverse crime* (Wirgin 2004). The ERT forward calculation was then repeated over the inverted ρ_{med}. The obtained *inverted* responses were compared with the responses of the true models.

As for ERT, we compared true and inverted MALM responses. First, the true response was simulated with the 8 current sources overt the true (not inverted) ρ_{med}. Second, a MALM response was calculated over the inverted ρ_{med} and inverted to obtained the inverted CSD. Third, the obtained inverted CSD was used to forward calculate the inverted MALM response over the inverted ρ_{med}. True and inverted MALM responses were then compared.

Plant experiments

We performed hydroponic and soil experiments using maize and cotton plants. In all the plant experiments, the injection electrode was positioned in the plant stem at a height of 1 cm from the surface of the growth media.

For the hydroponic experiments, the plants were first grown in columns with aerated nutrient solution (Hoagland and Arnon 1950). They were then moved to

the rhizotron for the experiments. As in the metallic roots test, the rhizotron was filled 1 day before the experiment to reach stable and homogeneous temperature and salinity conditions. The plant was positioned at the center of the rhizotron with soft rubber supports. The plants were submerged at the same level as in the growing column to avoid discrepancies caused by the plant tissue adaptation to the submerged and aerated conditions, as discussed above with regard to the growing conditions. Consequently, the root crown was approximately 3 cm below the water surface.

For the soil experiments, seedlings were grown directly in the rhizotron to avoid damaging the roots and altering the root-soil interface. The soil was prepared by mixing equal volumes of sandy and clay natural soils acquired from an agricultural study site run by U.C. Davis, CA (Russell Ranch). The plants were irrigated with double strength Hoagland solution (Hoagland and Arnon 1950).

Two soil experiments were performed. In the first experiment, four cotton plants were grown for four months. For these experiments, the plants were positioned with the root crown approximately 8 cm deep (y = 0.44 m). In the second experiment, a pregerminated maize seed was planted 3 cm deep and then grown for four months (Fig. 10).

Results

iCSD testing

Figure 3 shows the result of a synthetic numerical test performed to evaluate the iCSD resolution, inversion stability, and influence of imposed constraints. The obtained

CSD matches the true position of the simulated current source. The sum of the current sources equals 1 as expected and required by the continuity constraint. The resolution of the CSD is in line with the electrode interspace (5 cm). The first-order regularization (smoothness constraint) does not hinder the reconstruction of simulated point source.

Figure 4 shows the results of a laboratory experiment where the iCSD method was tested with a known distribution of current sources obtained with metallic wires. The use of metallic wires offered a comprehensive solution to test the overall correct functioning of the laboratory setup and inversion routine. The iCSD correctly characterized both position and intensity of the test sources with no need for prior information to constrain the solution. The asymmetrical distribution CSD agrees with the principle of path of least resistance, i.e., the closer to the return electrode, the shorter the water path, the higher the current source density. The obtained distribution of current source agrees with true CSD and resolution expected on the basis of previous numerical tests. The iCSD resolution was sufficient for the imaging of a root-like structure, e.g., differentiate between distal, proximal, or equally distributed current pathways in the roots (Fig. 4c). In this case, a distal CSD was investigated (tips of the metallic wires) and the iCSD correctly found no proximal current source (near the immersion point of the root-like metallic structure).

Figures 5, 6, and 7 show the results of the synthetic tests based on the 8-source laboratory tests. Figure 5 compares the true (a) and inverted (b) ρ_{med} to highlight the overall influence of rhizotron meshing, acquisition sequence, processing, and inversion. Figure 6a offers a more quantitative comparison between true and inverted ERT responses. Similarly, Fig. 6b presents the correlation between true iCSD response (true ρ_{med} and true CSD) and the inverted iCSD response (inverted ρ_{med} and inverted CSD). ERT and iCSD inverted responses correlate with the associated true responses (all correlation coefficients >0.95). Figure 7 shows the inverted CSD distribution and confirms the iCSD capability to characterize both intensity and position of the current sources with a resolution of 3 cm.

Plant Experimental Results.

The plant experiments investigated the root current pathways combining the iCSD with the direct observation of the roots. Hydroponic and soil experiments were performed with maize and cotton plants. Figure 8a shows the root architecture for one of the two plant hydroponic experiments with maize plants. Although the roots were visually observed to extend deeper in the rhizotron, both the inverted CSD distributions show that the current leakage in this hydroponic system primarily occurred in the proximal root part at the top of the rhizotron. In particular, the highest current density was predominantly concentrated near the root crown with the remaining current leakage already occurring along the submerged stem section. The ρ_{med} obtained from the ERT inversion confirmed the expected homogeneous temperature and salinity conditions.

In the soil experiments with cotton plants, the iCSD method successfully located the root position of the four plants along the soil surface and produced consistent signals corresponding to the root crowns (Fig. 9). The results also show a localized current leakage near the root crowns with no appreciable current leakage along the four stem sections in the soil or in the distal portions of the root systems. By contrast to the cotton results, the CSD distribution obtained from the maize experiment conducted within the soil presents current leakage along the stem section (Fig. 10).

The ERT-based ρ_{med} obtained from the cotton soil experiments presents a strong heterogeneity with a highly resistive layer at the top of the rhizotron, representing a dry soil layer (Fig. 9b). The evolution of this dry layer is due to water loss through evapotranspiration. The ERT results highlight the need to account for the heterogeneity of ρ_{med} in order to correctly calculate the responses of the VRTes during the iCSD. The ERT results also show how the ERT characterization can support the interpretation of the iCSD results by providing information on the soil characteristics and thus on possibly associated physiological responses, such as drought and suberization.

iCSD routine results

Both numerical and laboratory iCSD tests successfully image the CSD without requiring prior assumptions on the actual distribution of the roots and CSD. These assumptions were present in previous works (e.g., Mary et al. 2018) but were here replaced by application-specific constraints (smoothness, charge conservation, and positivity). In this sense, not only the explicit linear formulation allowed a direct implementation and evaluation of the these constraints, but also enabled full characterization of the resulting liner problem (e.g., condition

Fig. 6 Correlations between ERT true and inverted responses (**a**), and MALM true and inverted responses (**b**). A homogeneous resistivity of 10 Ω m was used for the homogeneous tests; a linear increment of the resistivity from 10 to 100 Ω m (bottom to top) was used for the linear tests; a quadratic increment of the resistivity from 10 to 750 Ω m was used for the quadratic test (Fig. 5). All linear correlation coefficients >0.95
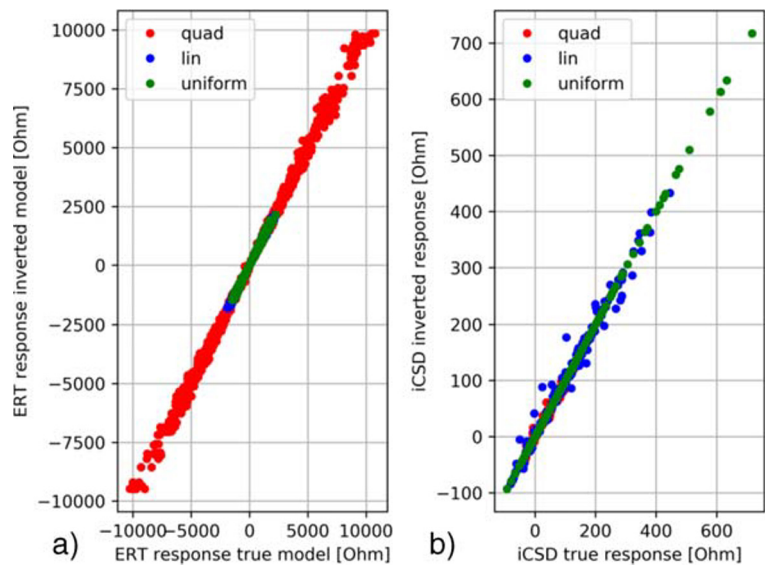

number, uncertainty analysis; see Strang (1976) and John (2015)).

Relative to the field setup of Mary et al. (2018), the laboratory setup offered the advantages of more flexible positioning of the electrodes and consequently better ERT and MALM data coverage. The other significant advantages over previous studies were the reduced number of VRTe in a 2D distribution and the new iCSD routine resulting from the 2D distribution of the VRTe and trans-dimensional ERT inversion.

The inversion times was significantly reduced by the proposed iCSD, particularly thanks to its

linear formulation, use of specific constraints and code optimization. Solving the linear system described above (Eq. 2) took less than 3 s on a standard laptop, compared to a few minutes using the generic optimization process used in Mary et al. (2018). The reduced inversion time also offers the advantage of a faster calculation of the Pareto front, which allowed a more informed inversion regularization.

Finally, the coupling between ERT and iCSD through the python geophysical library eased the optimization of the entire routine (Rücker et al. 2017). Coupling ERT

Fig. 7 CSD obtained from the 8-source numerical test with quadratic resistivity vertical profile (Fig. 5). The test is based on the laboratory experiment with metallic roots, see Fig. 4
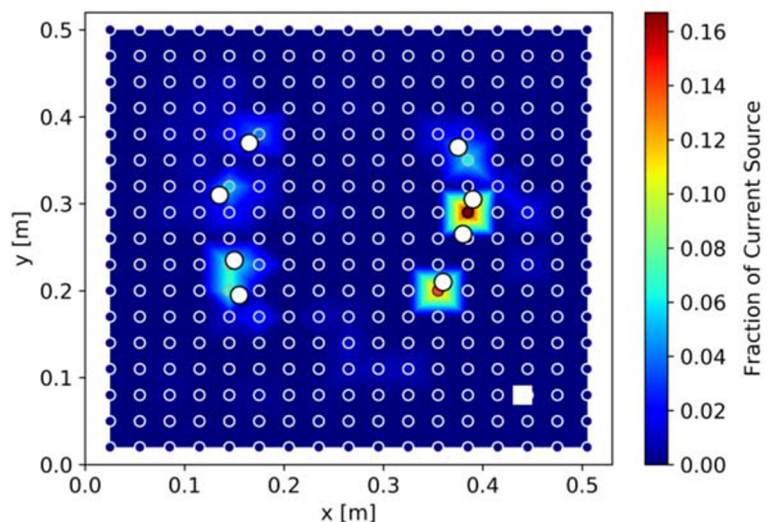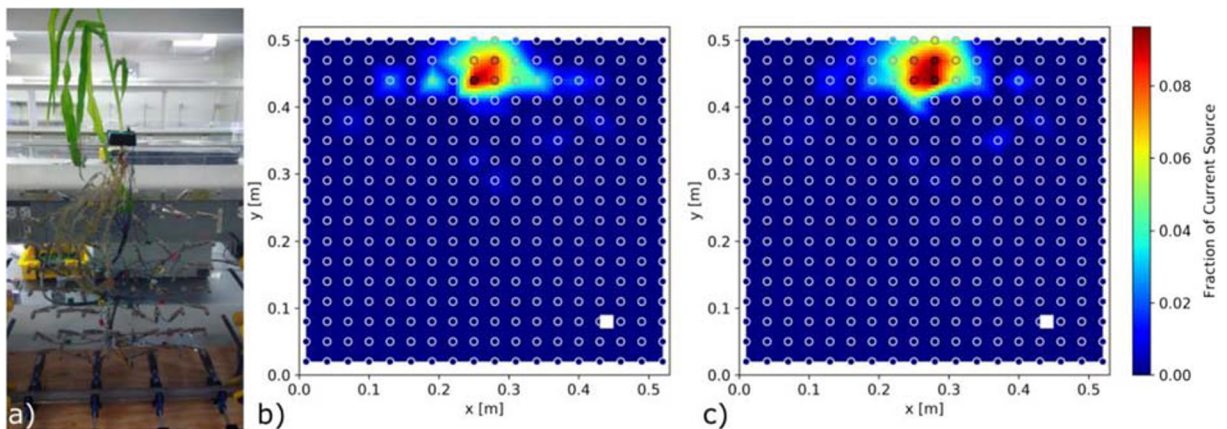
Fig. 8 Hydroponic experiments with a maize plant. a) Position of the plant and roots, with the root crown approximately 3 cm below the water surface. b-c) CSD obtained from the iCSD: the current leakage in proximal root part is dominant, while no appreciable current fraction reaches the distal part of the root system

and iCSD is a relevant aspect of our procedure because the ERT data processing/analysis routine has a strong influence on the successive iCSD inversion, which may require the entire procedure to be repeated to test different ERT inversion parameters (e.g., Fig. 9).

Discussion

The iCSD results showed that the current leakage occurred in the very proximal regions of the root systems in both soil and hydroponic conditions. The proximal leakage was observed despite the return electrode being placed at the bottom of the rhizotron to allow deep current pathways. Nonetheless, the expected influence of the return electrode position was observed in the laboratory test with metallic roots and motivates the use of this electrode configuration in future laboratory experiments.

Our results are consistent with the early studies on maize root electrical properties (Ginsburg 1972), and corroborate the recent works that questioned the assumptions of the BIA methods (Dietrich et al. 2012; Urban et al. 2011). The high resistivity of the top layer of soil (Fig. 9) is expected to induce root suberization (see Introduction): our results would support the physiological hypothesis of water and nutrient absorption through older and possibly suberized roots (Aroca 2012; Kramer 1946).

It is worth noticing that the absence of current leakage along the section of the cotton stems in the top dry soil supports the assumption that the electrical structure of roots controls their current conduction behavior. Suberized epidermal cells can affect the movement of ions and, consequently, the current conduction in roots (Cseresnyés et al. 2013; Čermák et al. 2006). Therefore, it is feasible for current to be conducted along deeper portions of the more woody roots with minor leakage. The BIA experimental results that have observed positive correlations between electrical signals and root area are likely a result of physiological correlations between the root regions that contribute to the current flow and hair roots, which contributes most to functional root surface area (Fig. 1c). While correlations between BIA electric signals and investigated root traits appear to be indirect, the correlations observed across experimental platforms and species continue to validate its value for in-situ root phenotyping (Dietrich et al. 2012).

In their study on field grapevines, Mary et al. (2018, 2019, 2020) concluded that the CSD could be used to infer the root depth distribution. Because of the significant suberization of major roots in grapevines and orange trees, the electric current could penetrate deep into the root system before significant leakage occured. The deeper current penetration allowed the iCSD method to access and phenotype the root system. On the contrary, limited current results in lower sensitivity of the iCSD to distal and younger parts of the root system that are likely dominated by less suberized, finer roots. We attribute
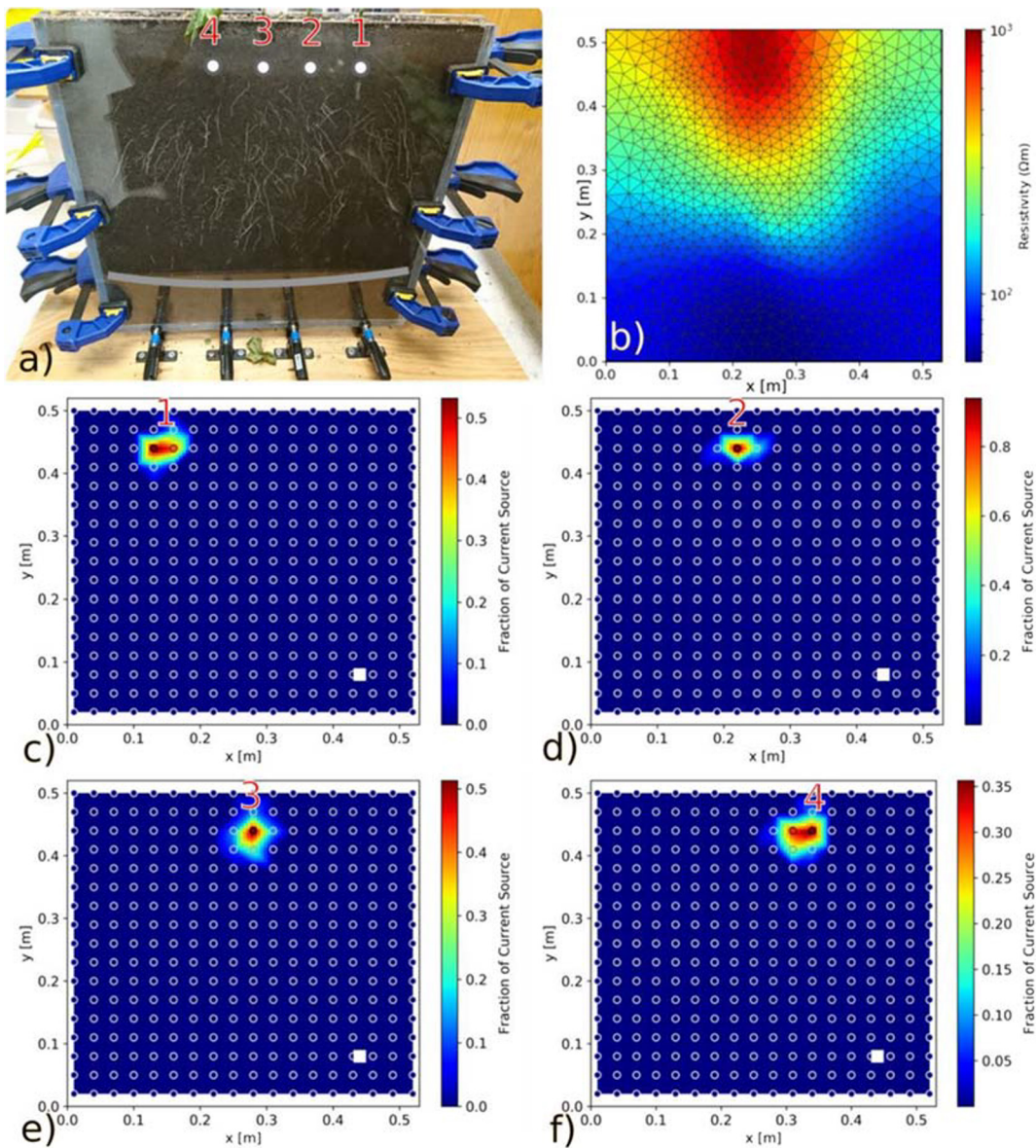
Fig. 9 Experiment with four cotton plants in soil. a) Rhizotron at the moment of the experiment with the root architectures and the dry soil layer at the top. The root crowns were approximately 8 cm deep (white dots). The gray line highlights the extension of the roots. b) ρ_{med} obtained from the ERT inversion highlighting the strong variability of the soil resistivity that has to be taken into account for a proper iCSD. ρ_{med} also confirms the presence of the top dry layer visible in a), which is caused by the evapotranspiration. c-g) iCSD results, in all the four experiments the current leakage concentrates near the root crown with no leakage along the stem above

differences in current penetration among root systems of maize, cotton, grapevine, and orange tree to the differences in physiological traits such as the extent of suberization and lignification. If on one hand the sensitivity to the root physiological traits is a promising opportunity, on the other hand it has to be accounted for when phenotyping more herbaceous roots.

Conclusions

In this study we present a novel numerical inversion routine for inversion of current source density in a bounded and non-homogeneous medium. The new inversion procedure offers an explicit matrix formulation that takes advantage of the problem
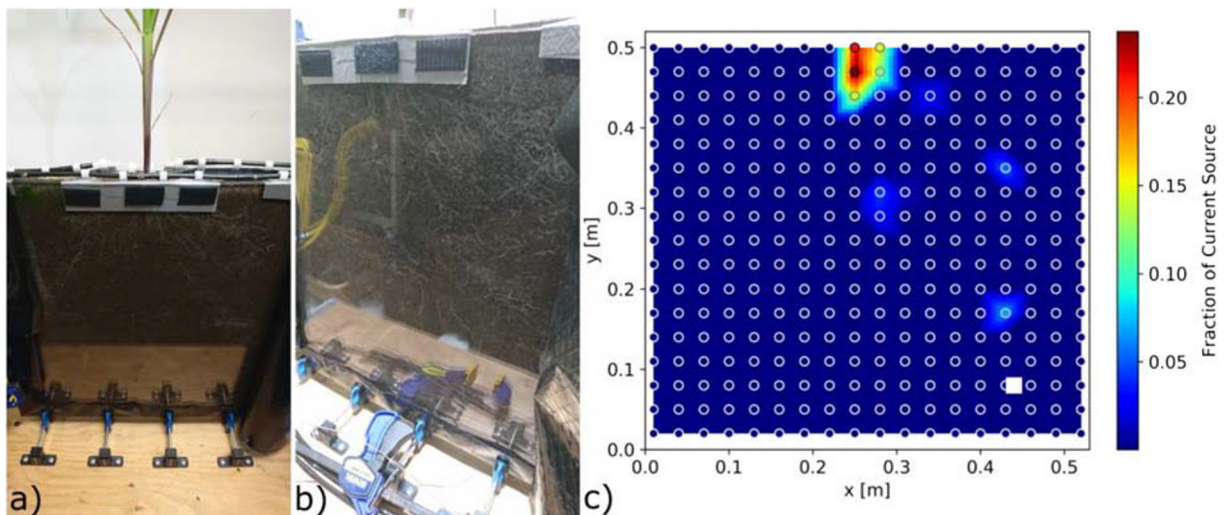
Fig. 10 Soil experiment with maize plant. a) and b) show the plant and root architecture at the moment of the experiment: the roots reach the bottom and sides of the rhizotron. c) iCSD result, the current passes from roots to soil in the most proximal part of the root system, with significant contribution from the stem section in the soil

linearity and constraints. The improvements provided by our numerical inversion technique enable a faster and more controlled imaging of the current source density. The numerical inversion routine was also coupled with an existing ERT inversion code to ease the overall inversion procedure. The iCSD inversion code was based on top of an open source geophysical Python library (Rücker et al. 2017).

After testing the method using synthetic numerical and laboratory experiments, we designed a specific rhizotron setup for laboratory plant experiments with maize and cotton. We found that with the obtained electrical coverage, the iCSD correctly characterized the different CSD distributions used in the tests, including the imaging of a root-like structure (Figs. 4, 6, and 7). By contrast to the results reported by Mary et al. (2018), the experimental setup and the new numerical inversion procedure did not require prior assumptions on the root distribution to stabilize and regularize the inversion. By eliminating the need for imputing prior information, our inversion protocol excludes the possibility of obtaining biased solutions.

In all seven plant experiments, the current left the root pathway in its proximal portion, radially leaking into the surrounding growth medium. These results corroborate recent studies that questioned the BIA assumptions (Urban et al. 2011; Dietrich et al. 2012). While these studies provided a thoughtful discussion

on the topic, they were based on time-consuming, invasive and less direct observations that restricted the ability to elucidate the complexity of root types and adaptation (e.g., excavation and trimming). This study describes the first direct and concurrent characterization of the root-soil current pathway and root architecture. Intrinsic differences in the root electrical properties of maize, cotton, grapevines, and orange trees emerge from the combined interpretation of our results with those presented by Mary et al. (2018, 2019), and Mary et al. 2020).

The laboratory rhizotron setup offered significant advantages for the development of the iCSD approach. Such advantages include the attainment of optimal electric coverage, direct root observation, and prior information on the growing medium. However, the development of the iCSD approach is well-timed and in line with the development of the geoelectrical technology for field-scale agricultural applications. The technological development driven by the use of ERT and SIP can readily be transferred to the iCSD approach. For example, the increased use of borehole electrodes and resistivity meter capabilities allow high electric coverage at the field-scale. The implementation of long-term monitoring has also become more common and provides precious information to characterize the dynamics of soil and vegetation. In this sense, the iCSD is a non-invasive solution that could be used to monitor the changes in root current pathways in response to water

stress and other environmental factors. In conclusion, our inversion approach fills a major gap toward the full implementation of methods that allow non-destructive imaging of roots in their natural soil environment.

References

Anderson WP, Higinbotham N (1976) Electrical resistances of corn root segments. Plant Physiol 57(2):137–141

Aroca R (2012) Plant responses to drought stress. Springer, Berlin

Atkinson JA, Pound MP, Bennett MJ, Wells DM (2019) Uncovering the hidden half of plants using new advances in root phenotyping. Curr Opin Biotechnol 55(1–8):1–8

Aubrecht L, Stanek Z, Koller J (2006) Electrical measurement of the absorption surfaces of tree roots by the earth impedance method: 1. Theory Tree Physiology 26(9):1105–1112

Binley A, Kemna A (2005) Electrical methods. In: Rubin Y, Hubbard SS. Hydrogeophysics. Springer, 441–463

Binley A, William D, Abelardo R (1997) Detecting leaks from environmental barriers using electrical current imaging. J Environ Eng Geophys 2:11–19

Bochev P, Lehoucq RB (2005) On the finite element solution of the pure Neumann problem*. SIAM Rev 47(1):50–66

Cao Y, Repo T, Silvennoinen R, Lehto T, Pelkonen P (2010) An appraisal of the electrical resistance method for assessing root surface area. J Exp Bot 61(9):2491–2497

Cassiani G, Boaga J, Vanella D, Perri MT, Consoli S (2015) Monitoring and modelling of soil–plant interactions: the joint use of ERT, sap flow and eddy covariance data to characterize the volume of an orange tree root zone. Hydrol Earth Syst Sci 19(5):2213–2225

Čermák J, Cudlín P, Gebauer R, Børja I, Martinková M, Staněk Z, Koller J, Neruda J, Nadezhdina N (2013) Estimating the absorptive root area in Norway spruce by using the common direct and indirect earth impedance methods. Plant Soil 372(1–2):401–415

Čermák J, Ulrich R, Staněk Z, Koller J, Aubrecht L (2006) Electrical measurement of tree root absorbing surfaces by the earth impedance method: 2. Verification based on allometric relationships and root severing experiments. Tree Physiol 26(9):1113–1121

Cseresnyés I, Rajkai K, Vozáry E (2013) Role of phase angle measurement in electrical impedance spectroscopy. Int Agrophys 27(4):377–383

Cseresnyés I, Szitár K, Rajkai K, Füzy A, Mikó P, Kovács R, Takács T (2018) Application of electrical capacitance method for prediction of plant root mass and activity in field-grown crops. Front Plant Sci 9:1–11

Dalton FN (1995) In-situ root extent measurements by electrical capacitance methods. Plant Soil 173(1):157–165

Dietrich RC, Bengough AG, Jones HG, White PJ (2012) A new physical interpretation of plant root capacitance. J Exp Bot 63(17):6149–6159

Enstone DE, Peterson CA (2005) Suberin lamella development in maize seedling roots grown in aerated and stagnant conditions. Plant, Cell and Environment 28(4):444–455

Findlay GP, Hope AB (1976) Electrical properties of plant cells: methods and findings. In: Lüttge U, Pitman MG (eds) Transport in plants II, Part A – Cells. Springer-Verlag, Berlin, pp 53–92

Fensom DS (1965) On measuring electrical resistance in situ in higher plants. Can J Plant Sci 46:169–175

Frensch J, Steudle E (1989) Axial and radial hydraulic resistance to roots of maize (Zea mays L.). Plant Physiol 91(2):719–726

Ginsburg H (1972) Analysis of plant root electropotentials. J Theor Biol 37(3):389–412

Günther T, Rücker C (2013) boundless electrical resistivity tomography BERT 2 - the user tutorial (august 8, 2013)

Günther T, Rücker C, Spitzer K (2006) Three-dimensional modelling and inversion of dc resistivity data incorporating topography - II. Inversion Geophys J Int 166(2):506–517

Guo L, Chen J, Cui X, Fan B, Lin H (2013) Application of ground penetrating radar for coarse root detection and quantification: a review. Plant Soil 362(1–2):1–23

Hacke UG, Sperry JS (2001) Functional and ecological xylem anatomy. Perspect Plant Ecol Evol Sys 4(2):97–115

Hansen PC, Dianne PO (1993) The use of the L-curve in the regularization of discrete ill-posed problems. SIAM J Sci Comput 14(6):1487–1503

Hoagland DR, Arnon DI (1950) The water-culture method for growing plants without soil. Circular California agricultural experiment station 347

Jackson RB, Sperry JS, Dawson TE (2000) Root water uptake and transport: using physiological processes in global predictions. Trends Plant Sci 5(11):482–488

John D (2015) Calibration and uncertainty analysis for complex environmental models. Watermark Numerical Computing, Brisbane

Johnson B (2013) The ascent of sap in tall trees: a possible role for electrical forces. Water 5:86–104

Knipfer T, Fricke W (2010) Root pressure and a solute reflection coefficient close to unity exclude a purely apoplastic pathway of radial water transport in barley (Hordeum vulgare). New Phytol 187(1):159–170

Kramer JP (1946) Absorption of water through suberized roots of trees. Plant Physiol 21(1):37–41

Łęski S, Pettersen KH, Tunstall B, Einevoll GT, Gigg J, Wójcik DK (2011) Inverse current source density method in two dimensions: inferring neural activation from multielectrode recordings. Neuroinformatics 9(4):401–425

Liu X, Dong X, Xue Q, Leskovar DI, Jifon J, Butnor JR, Marek T (2018) Ground penetrating radar (GPR) detects fine roots of agricultural crops in the field. Plant Soil 423(1–2):517–531

Maherali H, Pockman WT, Jackson RB (2009) Adaptive variation in the vulnerability of Woody plants to xylem cavitation. Ecology 85(8):2184–2199

Mancuso S (2012) Measuring roots. Springer, Berlin

Mary B, Peruzzo L, Boaga J, Schmutz M, Wu Y, Hubbard SS, Cassiani G (2018) Small scale characterization of vine plant root water uptake via 3D electrical resistivity tomography and Mise-A-La-masse method. Hydrol Earth Syst Sci Discuss 22(10):5427–5444

Mary B, Vanella D, Consoli S, Cassiani G (2019) Assessing the extent of citrus trees root apparatus under deficit irrigation via multi-method geo-electrical imaging. Sci Rep 9:9913

Mary B, Peruzzo L, Boaga J, Cenni N, Schmutz M, Wu Y, Hubbard SS, Cassiani G (2020) Time-lapse monitoring of root water uptake using electrical resistivity tomography and Mise-à-la-masse: a vineyard infiltration experiment. SOIL 6: 95–114

Menke W (1989) geophysical data analysis: discrete inverse theory. International Geophysics Series. Academic Press, New York

Minsley BJ, Sogade J, Morgan FD (2007) Three-dimensional source inversion of self-potential. J Geophys Res 112(B02202):1–12

North GB, Baker EA (2007) Water uptake by older roots: evidence from desert succulents. HortScience 42(5):1003–1006

Ozier-Lafontaine H, Bajazet T (2005) Analysis of root growth by impedance spectroscopy (EIS). Plant Soil 277(1–2):299–313

Parasnis DS (1967) Three-dimensional electric mise-a-la-masse survey of an irregular lead-zinc-copper deposit in Central Sweden. Geophys Prospect 15:407–437

Parasnis DS (1988) Reciprocity theorems in geoelectric and geoelectromagnetic work. Geoexploration 25:177–198

Postic F, Doussan C (2016) Benchmarking electrical methods for rapid estimation of root biomass. Plant Methods 12(1):33

Preston GM, McBride RA, Bryan J, Candido M (2004) Estimating root mass in young hybrid poplar trees using the electrical capacitance method. Agrofor Syst 60(3):305–309

Ranathunge K, Schreiber L (2011) Water and solute permeabilities of Arabidopsis roots in relation to the amount and composition of aliphatic suberin. J Exp Bot 62(6):1961–1974

Rao S, Meunier F, Ehosioke S, Lesparre N, Kemna A, Nguyen F, Garré S, Javaux M (2018) A mechanistic model for electrical conduction in soil-root continuum: a virtual rhizotron study. Biogeosciences 1:1–28

Redjala T, Zelko I, Sterckeman T, Legué V, Lux A (2011) Relationship between root structure and root cadmium uptake in maize. Environ Exp Bot 71(2):241–248

Ronczka M (2016) Saltwater detection and monitoring using metal cased boreholes as long electrodes. Doctoral Thesis. https://doi.org/10.14279/depositonce-5131

Rücker C, Günther T, Spitzer K (2006) Three-dimensional modelling and inversion of dc resistivity data incorporating topography - I. Modelling Geophys J Int 166(2):495–505

Rücker C, Günther T, Wagner FM (2017) pyGIMLi: an open-source library for modelling and inversion in geophysics. Comput Geosci 109:106–123

Schlumberger C (1920) Etude sur la prospection electrique du sous-sol. Gauthier-Villars

Schreiber L (2010) Transport barriers made of cutin, suberin and associated waxes. Trends Plant Sci 15(10):546–553

Shanahan PW, Binley A, Whalley WR, Watts CW (2015) The use of Electromagnetic induction to monitor changes in soil moisture profiles beneath different wheat genotypes. Soil Sci Soc Am J 79(2):459–466

Slater L, Binley A, Versteeg R, Cassiani G, Birken R, Sandberg S (2002) A 3D ERT study of solute transport in a large experimental tank. J Appl Geophys 49(4):211–229

Steudle E (2000) Water uptake by roots: effects of water deficit. J Exp Bot 51(350):1531–1542

Strang G (1976) Linear algebra and its applications. Academic press Inc, New York fourth edition

Tavakkoli E, Rengasamy P, McDonald GK (2010) The response of barley to salinity stress differs between hydroponic and soil systems. Funct Plant Biol 37(7):621

Trachsel S, Kaeppler SM, Brown KM, Lynch JP (2011) Shovelomics: high throughput phenotyping of maize (Zea mays L.) root architecture in the field. Plant Soil 341(1–2): 75–87

Urban J, Bequet R, Mainiero R (2011) Assessing the applicability of the earth impedance method for in situ studies of tree root systems. J Exp Bot 62(6):1857–1869

Weigand M, Kemna A (2017) Multi-frequency electrical impedance tomography as a noninvasive tool to characterize and monitor crop root systems. Biogeosciences 14:921–939

Weigand M, Kemna A (2019) Imaging and functional characterization of crop root systems using spectroscopic electrical impedance measurements. Plant Soil 435(1–2):201–224

Whalley W, Binley A, Watts C, Shanahan P, Dodd I, Ober E, Ashton R, Webster C, White R, Hawkesford MJ (2017) Methods to estimate changes in soil water for phenotyping root activity in the field. Plant Soil 415(1–2):407–422

Wirgin A (2004) The inverse crime. arXiv:math-ph/0401050

Zimmermann HM, Steudle E (1998) Apoplastic transport across young maize roots: effect of the exodermis. Planta 206:7–19